



Vibration isolation via a scissor-like structured platform



Xiuting Sun^{a,c}, Xingjian Jing^{a,b,*}, Jian Xu^c, Li Cheng^a

^a Department of Mechanical Engineering, Hong Kong Polytechnic University, Hong Kong, People's Republic of China

^b Shenzhen Research Institute of Hong Kong Polytechnic University, Shenzhen, People's Republic of China

^c School of Aerospace Engineering and Applied Mechanics, Tongji University, Shanghai, People's Republic of China

ARTICLE INFO

Article history:

Received 4 July 2013

Received in revised form

2 December 2013

Accepted 26 December 2013

Handling Editor: H. Ouyang

Available online 28 January 2014

ABSTRACT

More and more attentions are attracted to the analysis and design of nonlinear vibration control/isolation systems for better isolation performance. In this study, an isolation platform with n -layer scissor-like truss structure is investigated to explore novel design of passive/semi-active/active vibration control/isolation systems and to exploit potential nonlinear benefits in vibration suppression. Due to the special scissor-like structure, the dynamic response of the platform has inherent nonlinearities both in equivalent damping and stiffness characteristics (although only linear components are applied), and demonstrates good loading capacity and excellent equilibrium stability. With the mathematical modeling and analysis of the equivalent stiffness and damping of the system, it is shown that: (a) the structural nonlinearity in the system is very helpful in vibration isolation, (b) both equivalent stiffness and damping characteristics are nonlinear and could be designed/adjusted to a desired nonlinearity by tuning structural parameters, and (c) superior vibration isolation performances (e.g., quasi-zero stiffness characteristics etc.) can be achieved with different structural parameters. This scissor-like truss structure can potentially be employed in different engineering practices for much better vibration isolation or control.

© 2014 Elsevier Ltd. All rights reserved.

1. Introduction

An excellent vibration isolation system can be applied widely in engineering practice such as vehicle suspension systems [1], protection of high-precision machinery [2], space launch or on-orbit vibration isolation [3] and so on. To suppress vibration over a larger frequency range, an isolator so-called quasi-zero-stiffness vibration isolator (QZS-VI) is proposed and studied in the literature [2], [4–11]. It can realize ultra-low stiffness [2], [5–9], zero stiffness [4], or negative stiffness [10,11] characteristics by designing structural parameters. The QZS-VIs can achieve vibration suppression over a broad frequency band, and thus remove major disadvantages of traditional linear vibration isolator systems. Even for the problems such as large static displacement and low static stiffness of the QZS-VIs, they can also be overcome by introducing some structural or control nonlinearity [6], [9–11]. However, strong nonlinear stiffness can induce strong nonlinear behaviors such as jumping and bifurcation. Moreover, obvious disadvantages for the class of QZS-VIs are the easiness to lose stability, low loading capability and potential bifurcation effect at equilibrium incurred by negative linear stiffness [10], [11]. Therefore, structural parameters of the QZS-VIs must be carefully designed in order to realize QZS characteristics with better loading capacity and stability.

* Corresponding author.

E-mail addresses: xingjian.jing@polyu.edu.hk, xingjian.jing@gmail.com (X. Jing).

In order to achieve excellent vibration isolation, better loading capacity and simultaneously more robustness in stability control, there are many vibration control systems utilizing active control strategies in the literature. Usually, to reduce the vibration at resonant frequency is to increase the value of damping coefficient. An increase of linear damping is effective at resonant frequency but not for other frequencies and even worse for high frequencies. Some recent studies indicate that nonlinear damping is effective both for low and high frequencies [12–14,26]. Therefore, magneto-rheological fluid (MRF) dampers, as a smart and controllable liquid material, are extensively studied for achieving adjustable nonlinear damping characteristics in vibration suppression [15], [17–20]. The application of MRF dampers is thus investigated by many researchers in various vibration controls such as rotor support systems and vehicle suspension [16–18,22].

Beneficial nonlinear stiffness and damping characteristics can also be obtained through active control. It is found that combining classical sky-hook feedback with a feed-forward control can obtain damping improvement [21]. Zapateiro et al. [22] design a semi-active controller for a class of vehicle suspension system utilizing MR damper. Some research results employ H -infinite control theory for active control of vehicle suspension systems considering actuator delay and fault [23,24]. Noticeably, the time delay in control input can also be used as a critical factor to tune system nonlinear dynamic response and thus to achieve better vibration control performance [25,31]. A delayed-resonator vibration absorber is first proposed by Olgac [27–29]. To broaden a valid range in frequency for suppression of vibrations, Zhao et al. [30] proposed a delayed-resonator vibration absorber with nonlinear master and slave structures. Bhikkaji et al. [31] used integral resonant control to damp the vibration of a collocated structure and corresponding experiment proved the effect of the control strategy. There are also several results designing truss structure to obtain better vibration isolation. The authors in [32] present a seat suspension system with one-layer truss. Then an active control device in an air spring assembled in this suspension system is studied in [33]. It is demonstrated that the active control results in about 50 percent reduction of the vibration compared with the passive one around the resonant frequency. It should be noted that, active control methods for vibration isolation or suppression might not be preferable in practice because of its high energy cost and construction/installation expense.

In this study, a versatile n -layer scissor-like structured vibration isolation (SLS-VI) platform is proposed to explore new design of nonlinear vibration isolation systems (preferable in passive and/or semi-active control manners). The nonlinearity of the SLS platform is induced by geometrical relationship of the structure, which is shown to be very helpful to equilibrium stability. It is demonstrated that this SLS-VI platform can overcome major disadvantages of traditional spring–mass–damping vibration isolators, the existing QZS-VI systems and active control vibration isolation systems mentioned above. The proposed SLS-VI system can achieve superior nonlinear vibration isolation using only pure linear elements in the system with a simple and flexible installation structure, can realize adjustable nonlinear damping and stiffness design with different structural parameters, and thus can provide better vibration isolation performance for many engineering practices. The contributions of this study mainly lie in the following 3 points: (a) It is shown for the first time that the SLS platform is a very versatile and beneficial system which can achieve much better QZS property in vibration isolation; (b) The nonlinear properties of the scissor-like structure are very beneficial in vibration isolation/control, which can be easily designed by tuning structure parameters; (c) It is demonstrated that the scissor-like structure is a very ideal, novel, and passive solution to realization of beneficial nonlinear stiffness and damping characteristics in vibration isolation/control. To demonstrate the advantages of the SLS-VI system, comparisons with those existing vibration isolation methods mentioned above are given and discussed.

The paper is organized as follows. Firstly, the SLS-VI platform is introduced in Section 2. The rotational friction of every joint of the truss structure and linear horizontal friction are taken into consideration for the modeling. Secondly, to compare the isolation effect, the isolation effects for different structural parameters are shown in Section 3. Then, the mechanism of isolation of the platform is discussed in Section 4. The platform can achieve better weight capacity and excellent vibration isolation performance since the structural parameters can effectively change the equivalent stiffness and damping of the system. Finally, a conclusion is given in Section 5.

2. The n -layer SLS-VI platform and its modeling

Consider the SLS-VI platform with n -layer truss structure in this section. A 3-layer SLS-VI system is shown in Fig. 1, subjected to the base excitation. Each layer of the truss is scissor-like and constructed by connecting rods and corresponding rotating joints. The supporting joints in the left bottom and top layer are free sliding along pre-designed horizontal tracks. Obviously, the properties of contacting surface on these sliding tracks and in rotating joints can be designed for different damping properties. Potentially, some springs can be used as indicated to achieve the stiffness of the system.

Because the platform is symmetric, the modeling of the system can be simplified to a plane problem as shown in Fig. 2, which is the front view of the isolation platform with n -layer truss structure. The mass of the isolation object is denoted by M . The connecting rods have the same length denoted by $2l$ and the assembly angle with respect to the horizon line is represented by θ . More practically, the stiffness of the springs is supposed to satisfy a property $f=k_1(\cdot)+k_n(\cdot)^3$. The air damping effect is also considered with a property $f=c_1 \cdot d(\cdot)/dt$. All the structural parameters are listed in Table 1 in Appendix A.

The absolute motion of the mass M is denoted by y , the base excitation z , the rotation angle of each connecting rod φ , and the horizontal motion of the left support joint at the bottom layer x . The positive direction of the motion y is upward as shown in Fig. 2. All motion variables are listed in Table 2 in Appendix A.

The rotation motion of each rod φ is shown in Fig. 3. The connecting rods can be designed to much lighter in weight compared with the isolation mass, sufficiently short in length and strong in stiffness (via choosing materials, e.g., steel or

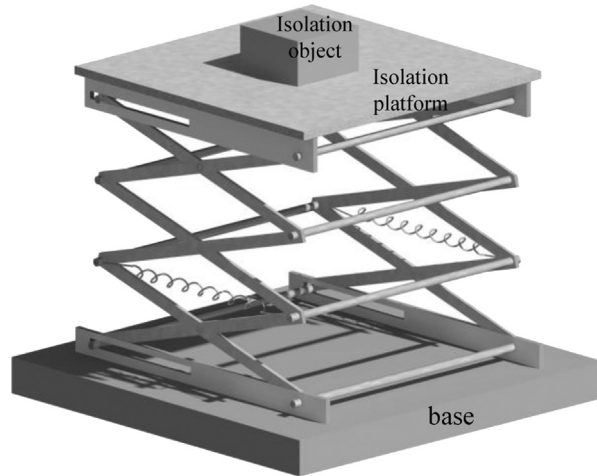


Fig. 1. The 3-layer SLS-VI platform.

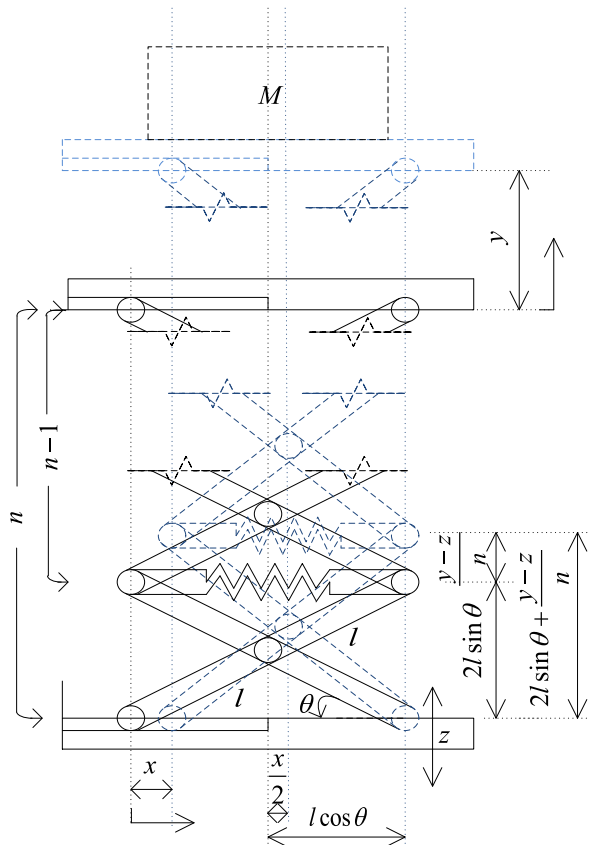


Fig. 2. The *n*-layer SLS-VI platform in modeling.

carbon fiber etc) to reduce potential inertia or flexibility influence in dynamic response. For convenience in discussion and for understanding dominant dynamic response of the system, the mass of the connecting rods are not considered in system modeling of this study. Without considering the mass of connecting rods in the truss structure, the dynamic equation of the system can be obtained by Lagrange principle. The absolute motion of the isolation object y is the generalized coordinate. Considering the friction of each connecting joint, the kinetic energy can be written as

$$T = \frac{1}{2} M \dot{y}^2 \tag{1}$$

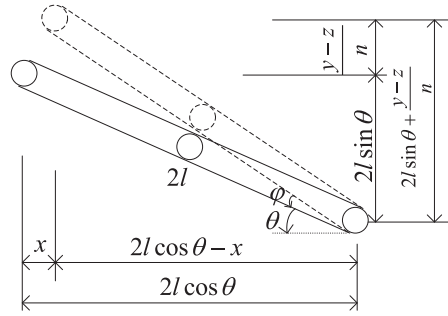


Fig. 3. The motion of one connecting rod in the first layer.

and the potential energy as

$$V = \frac{1}{2}k_1x^2 + \frac{1}{4}k_nx^4 \tag{2}$$

The Lagrange principle is as

$$\frac{d}{dt} \left(\frac{\partial L}{\partial \dot{y}} \right) - \frac{\partial L}{\partial y} = -D_1 - D_2 - D_3 \tag{3}$$

where L is the Lagrange function expressed as $L=T-V$, D_1 the dissipated energy for air damping, D_2 the dissipated energy due to structural rotational friction and D_3 the dissipated energy due to horizontal friction. It can be obtained that

$$D_1 = c_1(\dot{y} - \dot{z}) \tag{4}$$

$$D_2 = n_x c_2 \dot{\varphi} \tag{5}$$

$$D_3 = c_3 \dot{x} \tag{6}$$

where c_1 is the air damping coefficient, c_2 the rotational friction coefficient of each joint, c_3 the damping coefficient of horizontal motion and n_x is defined as the number of joints which provides rotational friction. From (4–6), the effect of the friction in this isolation platform is to suppress or dissipate the vibration energy and the function of D_2 and D_3 are all linear functions of the motion φ and x .

From Fig. 2 and Fig. 3, because the relative motion between the mass M and the base is $\hat{y}=y-z$ where y is the absolute motion of the mass M and z the base excitation, the geometrical relation of variables φ , x and \hat{y} can be obtained as

$$\tan(\varphi + \theta) = \frac{2l \sin \theta + \hat{y}/n}{2l \cos \theta - x} \tag{7}$$

and

$$(2l)^2 = \left(2l \sin \theta + \frac{\hat{y}}{n} \right)^2 + (2l \cos \theta - x)^2 \tag{8}$$

From (7) and (8), the transport motion φ and x are expressed as

$$\varphi = \arctan \left[\frac{2l \sin \theta + \hat{y}/n}{2l \cos \theta - x} \right] - \theta \tag{9}$$

and

$$x = 2l \cos \theta - 2\sqrt{l^2 - (l \sin \theta + \hat{y}/2n)^2} \tag{10}$$

The transport motion φ and x are shown in Fig. 4 for $n=2$, $l=0.5$, and $\theta=\pi/4$.

It shows clearly in Fig. 4 the nonlinear relationships among the transport motion x , φ and \hat{y} . Note that there are rotational frictions in the rotational joints of each connecting rod, and there are totally six joints in each layer. Thus $n_x=6n$ in (5) where n is the number of layers. By substituting kinetic energy (1), potential energy (2), friction functions in (4–6) and transport motion (9) and (10) into the Lagrange principle (3), the dynamic equation of the SLS-VI platform can be obtained as

$$M\ddot{y} + (k_1x + k_nx^3) \frac{dx}{d\hat{y}} \frac{d\hat{y}}{dt} = -c_1(\dot{y} - \dot{z}) - n_x c_2 \dot{\varphi} - c_3 \dot{x} \tag{11}$$

where $\dot{\varphi} = (d\varphi/d\hat{y}) \cdot (d\hat{y}/dt)$ and $\dot{x} = (dx/d\hat{y}) \times (d\hat{y}/dt)$ because of (9) and (10). Substitute $\hat{y}=y-z$ into (11) and define f_1, f_2, f_3 for the stiffness, rotational friction of joints and horizontal friction as

$$f_1(\hat{y}) = (k_1x + k_nx^3) \frac{dx}{d\hat{y}} \tag{12}$$

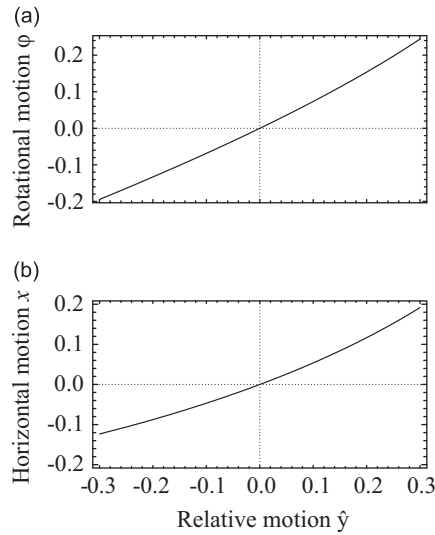


Fig. 4. The transport motion φ , x and \hat{y} for $n=2$, $l=0.5$, and $\theta=\pi/4$. (a) Relationship between \hat{y} and φ ; (b) relationship between \hat{y} and x .

$$f_2(\hat{y}) = \frac{d\varphi}{d\hat{y}} \tag{13}$$

$$f_3(\hat{y}) = \frac{dx}{d\hat{y}} \tag{14}$$

Then the dynamic equation containing the friction of the platform is

$$M\ddot{y} + f_1(\hat{y}) + c_1\dot{y} + n_x c_2 f_2(\hat{y})\dot{y} + c_3 f_3(\hat{y})\dot{y} = -M\ddot{z} \tag{15}$$

From (12–14), the expressions for f_1, f_2, f_3 can be further derived as

$$f_1(\hat{y}) = \frac{(\hat{y}/2n + l \sin \theta)(k_l x + k_n x^3)}{n\sqrt{l^2 - (l \sin \theta + \hat{y}/2n)^2}} \tag{16}$$

$$f_2(\hat{y}) = \frac{1}{\sqrt{4l^2 n^2 - (2ln \sin \theta + \hat{y})^2}} \tag{17}$$

$$f_3(\hat{y}) = \frac{\hat{y}/2n + l \sin \theta}{n\sqrt{l^2 - (\hat{y}/2n + l \sin \theta)^2}} \tag{18}$$

It can be seen that f_1, f_2, f_3 are continuous at $\hat{y}=0$. Therefore, f_1, f_2, f_3 can be expanded by Taylor series at zero equilibrium as

$$f'_1(\hat{y}) = \beta_1\hat{y} + \beta_2\hat{y}^2 + \beta_3\hat{y}^3 + \beta_4\hat{y}^4 \tag{19}$$

$$f'_2(\hat{y}) = \zeta_0 + \zeta_1\hat{y} + \zeta_2\hat{y}^2 \tag{20}$$

$$f'_3(\hat{y}) = \zeta_3 + \zeta_4\hat{y} + \zeta_5\hat{y}^2 \tag{21}$$

where the definition for $\beta_1, \beta_2, \beta_3, \beta_4, \zeta_0, \zeta_1, \zeta_2, \zeta_3, \zeta_4$, and ζ_5 are listed in (B.1–B.10) in Appendix B. When $k_n=0$, the stiffness property of the spring is a linear function $F=k_l(\cdot)$. For the case $k_l=1000, l=0.5, \theta=\pi/4$ and $n=2$, the Taylor series expansion f'_1, f'_2, f'_3 and original functions f_1, f_2, f_3 are compared in Fig. 5.

From Fig. 5, utilizing the Taylor series expansion, (19–21) can basically represent very well the mechanical properties of the original stiffness, rotational friction and horizontal friction of the platform. As $k_n=0$, it can be seen that the equivalent stiffness and damping properties are nonlinear functions while the spring and damper in the system are only linear functions of motion and velocity. It is clear that the equivalent nonlinear stiffness and damping are induced by the nonlinear geometrical relations among vertical, horizontal and rotational motions of this SLS platform. Also, Fig. 5 shows that the stiffness function and damping functions are asymmetric at zero. Therefore, the vibration response must be asymmetric at zero equilibrium, which requires the consideration of offset when using the harmonic balance method (HBM) [34]. It should also be noted (see Fig. 5) that the nonlinearities involved here are basically weakly nonlinear, which cannot induce

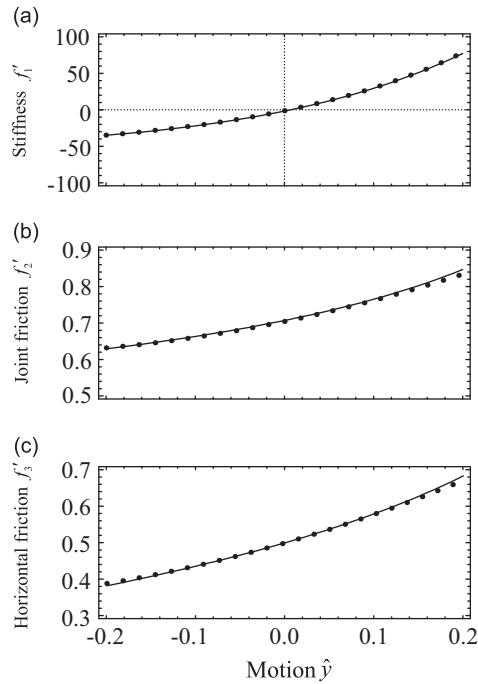


Fig. 5. Taylor expansion (dots) compared with original stiffness and friction functions (solid lines) of the platform (a) stiffness; (b) joint friction; and (c) horizontal friction.

bifurcation, multi-stable states or chaos, and thus will not bring stability problem to the system for small excitation or usual parameter setting. The analysis results with the harmonic balance method later will verify this clearly in Sections 3 and 4.

Substituting the Taylor series expansion (19)–(21) for f_1, f_2, f_3 into Eq. (15), the dynamic equation can be rewritten as

$$M\ddot{y} + n_x c_2 (\zeta_0 + \zeta_1 \dot{y} + \zeta_2 \dot{y}^2) \dot{y} + c_3 (\zeta_3 + \zeta_4 \dot{y} + \zeta_5 \dot{y}^2) \dot{y} + c_1 \dot{y} + \beta_1 \dot{y} + \beta_2 \dot{y}^2 + \beta_3 \dot{y}^3 + \beta_4 \dot{y}^4 = -M\ddot{z} \tag{22}$$

where the base excitation $z = z_0 \cos \omega_0 t$. The dimensionless parameters are introduced as Table 3 in Appendix A. Then dimensionless dynamic equation of (22) is given by

$$\hat{y}'' + \omega_2^2 \hat{y} + \gamma_1 \hat{y}^2 + \gamma_2 \hat{y}^3 + \gamma_3 \hat{y}^4 + 2\xi_1 \hat{y}' + 2\xi_2 \hat{y} \hat{y}' + 2\xi_3 \hat{y}^2 \hat{y}' = -z'' \tag{23}$$

where $(\cdot)' = d(\cdot)/dt'$. In (23), the equivalent stiffness and damping characteristics are asymmetric at zero equilibrium, which requires the consideration of zero offset when using the Harmonic Balance Method (HBM) [34] for theoretical results. The solution of (23) can be set as $\hat{y} = a_0 + a \cos(\Omega t' + \phi)$ where a_0 is the bias term and a is the amplitude of harmonic term. The equations for a_0 and a obtained by applying the HBM are provided by (C.1) and (C.2) in Appendix C. From (C.1)– in Appendix C and the condition $\sin^2 \phi + \cos^2 \phi = 1$, the displacement transmissibility T_d can be obtained as

$$T_d = \left| \frac{\sqrt{a^2 + z_0^2 + 2az_0 \cos \phi}}{z_0} \right| \tag{24}$$

where a and z_0 is the amplitude of relative vibration \hat{y} and the base excitation z .

3. Vibration isolation performance and its relationships with structural parameters

The structural parameters of the platform can be designed for different vibration isolation performance. The parameter layer n , assembly angle θ , damping coefficient c_3 induced by horizontal friction, and the length of connected rod l can all be considered as structural parameters to be designed for different vibration isolation performance, and others are supposed to be fixed in this study which are chosen as $k_l = 1000, k_n = 10000, c_1 = 5, c_2 = 1, M = 10, z_0 = 0.05$ and $n_x = 6n$. The displacement transmissibility T_d solved by (24) can be used to reflect the vibration isolation effect with different structural parameters.

3.1. Effect of layer number n

For $l = 0.5, \theta = \pi/4$ and $c_3 = 1$, the vibration isolation performance for different number of layer is shown in Fig. 6.

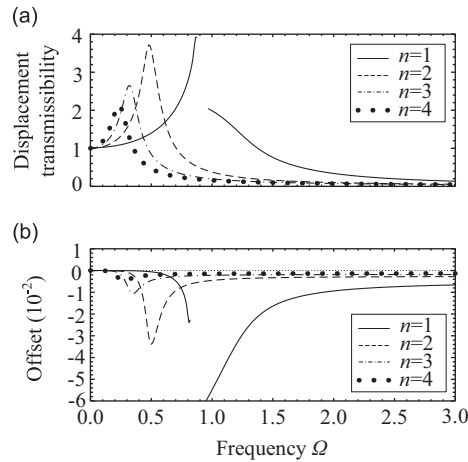


Fig. 6. The isolation performance for different n as $\theta=\pi/4$, $c_3=1$ and $l=0.5$. (a) The displacement transmissibility; and (b) The offset of the platform.

Fig. 6 shows that the isolation effect of the platform is obviously influenced by the number of layer n . It can be seen that increasing the number of the truss in the platform can improve the vibration isolation performance and reduce the offset value in the displacement of the mass M (due to the asymmetrical stiffness and damping).

In Fig. 6(a), for $n=1$ the resonant peak is large and there exists jumping phenomena both in the displacement transmissibility and offset. The curve left to the jumping area in the displacement transmissibility demonstrates a hard spring property while the right one soft spring property. The vibration amplitude for the soft spring characteristic is smaller than that in a similar case of a traditional linear system or a Duffing system. When $n=2$, the resonant frequency is reduced to 0.5 and the resonant peak becomes obviously smaller than that for $n=1$. The resonant frequency reduces to only about 0.25 for $n=4$ and the peak value keeps becoming smaller, demonstrating a quasi-zero-stiffness property. Therefore, the vibration isolation performance becomes better with the increase of the layer n .

In Fig. 6(b), the offset curve as $n=1$ reflects the nonlinear property of the system with a jumping phenomenon. The offset for $n=1$ demonstrates soft spring characteristic induced by the asymmetry terms in the dynamic equation. With the soft spring characteristic, the frequency range for jumping phenomena is smaller than that of isolators with hard spring characteristic. The offset is becomes only about 0.003 for $n=4$. Therefore, increasing the number of layers is helpful for reduction of the offset phenomenon.

3.2. Effect of assembly angle θ

The other parameters are fixed as $n=2$, $c_3=1$ and $l=0.5$. The displacement transmissibility for different value of assembly angle θ is shown in Fig. 7.

From Fig. 7, it can be seen that when θ is around or larger $\pi/3$, there is a jump phenomenon in the displacement transmissibility and offset curve demonstrating strong nonlinear behavior, while the displacement transmissibility and offset value both become smaller with the decrease of angle θ , intending to be a quasi-zero-stiffness property as well.

3.3. Effect of damping coefficient c_3

With the other parameters set to $n=2$, $\theta=\pi/4$ and $l=0.5$, the vibration isolation performance for different damping coefficient c_3 is shown in Fig. 8.

From Fig. 8, it can be seen that increasing the damping coefficient c_3 can obviously decrease the vibration transmissibility and the offset of the platform around resonant frequency, while almost does not affect both curves at low and high frequencies. Therefore, c_3 should be a critical parameter to reduce the vibration around resonant frequency.

It is known that an increase of the linear damping in a traditional spring–mass–damping isolator will improve vibration suppression around the resonant frequency but usually deteriorate the performance much at high frequencies. This does not happen to the proposed platform as shown in Fig. 8(a) due to the underlying equivalent nonlinear damping effect, which will be further discussed in Section 4.

3.4. Effect of length of connecting rod l

With the other parameters set to $n=2$, $\theta=\pi/4$ and $c_3=1$, the displacement transmissibility for different length l is shown in Fig. 9.

From Fig. 9(a), it can be seen that decreasing the length of connecting rod l can reduce the vibration transmissibility at around resonant frequency but almost brings no effect at low and high frequencies (slight reduction at low frequencies).

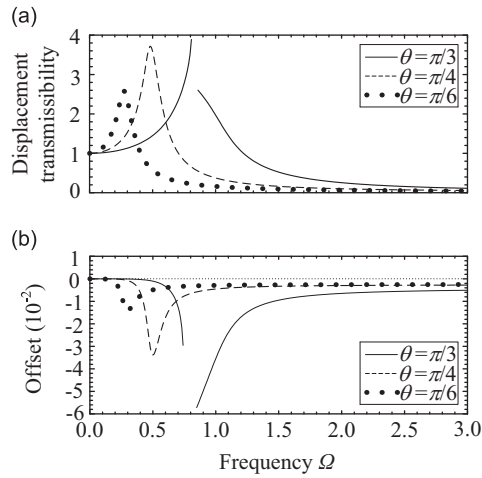


Fig. 7. The isolation performance for different θ as $n=2$, $c_3=1$ and $l=0.5$. (a) The displacement transmissibility; (b) The offset of the platform.

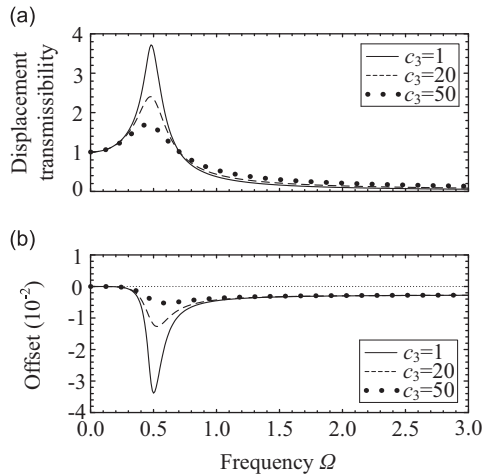


Fig. 8. The isolation performance for different damping coefficient c_3 for $n=2$, $\theta=\pi/4$ and $l=0.5$. (a) The displacement transmissibility; and (b) the offset of the platform.

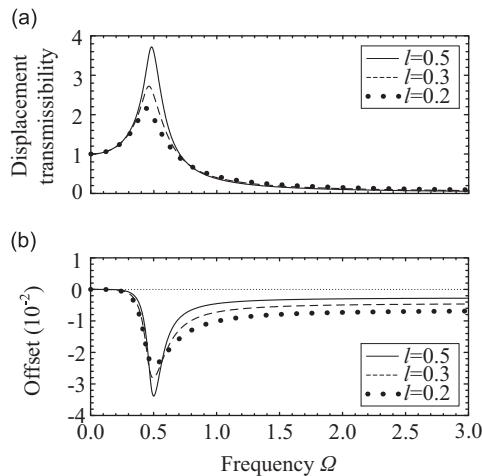


Fig. 9. The isolation performance for different length of connected rod l for $n=2$, $\theta=\pi/4$ and $c_3=1$. (a) The displacement transmissibility; and (b) the offset of the platform.

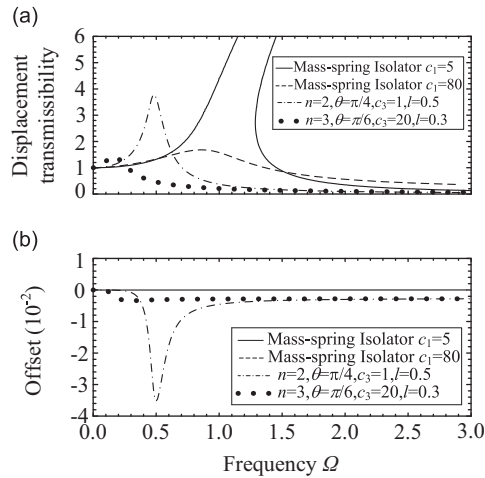


Fig. 10. The comparison with typical spring–mass–damping system for different structural parameters. (a) The displacement transmissibility; and (b) the offset of vibration.

This is very similar to the nonlinear damping effect mentioned previously. However, Fig. 9(b) shows that the decrease of the length l will increase obviously the offset value of the platform at high frequencies with a little reduction at around resonant frequencies.

Considering both Fig. 8 and Fig. 9, it can be concluded that the effects of l and c_3 on the vibration transmissibility are very similar, and both are very effective and advantageous. The damping coefficient c_3 has little effect on the vibration offset at high frequencies while the rod length l influences much.

3.5. Comparisons with some existing isolation systems

3.5.1. Typical spring–mass–damping isolators

For a traditional spring–mass–damping vibration isolator with mass M , a spring having linear stiffness k_l and nonlinear stiffness k_n , and damper with coefficient c_1 , its dynamic equation under base excitation z is given by

$$M\ddot{y} + k_l(y - z) + k_n(y - z)^3 + c_1(\dot{y} - \dot{z}) = 0 \tag{25}$$

Define the relative motion as $\hat{y} = y - z$ where $z = z_0 \cos \omega_0 t$ and the dimensionless parameters are as Table 4 in Appendix A, the dimensionless dynamic equation is

$$\hat{y}'' + \hat{y} + \gamma \hat{y}^3 + 2\xi \hat{y}' = -z'' \tag{26}$$

where $(\cdot)' = d(\cdot)/dt$. The solution of (16) can be set as $\hat{y} = a \cos(\Omega t + \phi)$. Then, the displacement transmissibility of the spring–mass–damping isolator can be obtained similarly by (24).

The vibration isolation performance of the SLS-VI platform is compared to that of the typical spring–mass–damping isolator system in (25). Use the same structural parameters as $k_l = 1000$, $k_n = 10,000$, $c_1 = 5$, $c_2 = 1$, $M = 10$, $z_0 = 0.05$, and $n_x = 6n$ for considering friction of each joint in each layer, the comparison results are shown in Fig. 10.

It can be seen clearly from Fig. 10(a) that the vibration transmissibility of the SLS-VI platform is much better than that of the typical spring–mass–damping isolator, although a little vibration offset exists for the SLS-VI platform. Firstly, the resonant frequency of the mass–spring–damping isolator is always around 1 while it can be reduced obviously for the SLS-VI by adjusting structural parameters such as n , θ and l . Secondly, the increase of the damping coefficient of the mass–spring–damping isolator for example $c_1 = 80$ can improve the isolation effect at resonant frequency, but greatly deteriorate the transmissibility at high frequencies. This is not true for the SLS-VI as mentioned before. Importantly, several structure parameters actually contribute to the equivalent stiffness and damping characteristics of the SLS-VI. This potentially provides a simple and very practical method for achieving different stiffness and damping characteristics in practice. This will be further investigated in Section 4.

3.5.2. Quasi-zero-stiffness isolators

The dynamic response of a quasi-zero-stiffness isolator [2], [4–11] under base excitation can be expressed as an oscillator with zero linear stiffness and cubic nonlinear stiffness as follows:

$$M\ddot{\hat{y}} + k_n \hat{y}^3 + c_1 \dot{\hat{y}} = -M\ddot{z} \tag{27}$$

With the dimensionless variables defined as Table 5 in Appendix A, the dimensionless equation is given by

$$\hat{y}'' + \gamma \hat{y}^3 + 2\xi \hat{y}' = -z'' \tag{28}$$

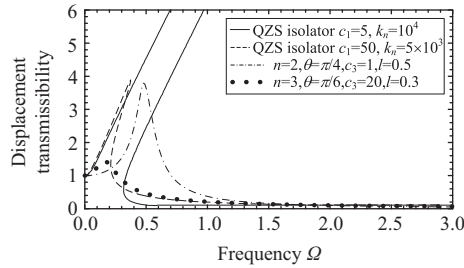


Fig. 11. The comparison with QZS isolators under different structural parameters.

where $(\bullet)' = d(\bullet)/dt$. The solution of the QZS isolator above also can be obtained by (24). Again, using the same structural parameters as $k_l = 1000$, $k_n = 10,000$, $c_1 = 5$, $c_2 = 1$, $M = 10$, $z_0 = 0.05$, and $n_x = 6n$, the comparison results are shown in Fig. 11.

From Fig. 11, the overall performance of the SLS-VI platform is very competitive and could be much better, compared with that of the QZS isolator. (a) By adjusting structural parameters, both isolators can achieve quasi-zero stiffness in vibration control. (b) To achieve a larger loading capacity, the nonlinear stiffness coefficient of the QZS should be larger. However, a larger stiffness coefficient would result in a multi-steady state phenomenon in a wider frequency range (as seen in Fig. 11), which is a very strong nonlinear response behavior and very dangerous (to lose stability) in vibration control. To ensure stability, the structural parameters of the QZS isolator should be in some critical ranges. The SLS-VI basically has no this strong nonlinear phenomenon (the jump behavior mentioned before can be easily avoided) and thus has no this stability problem. (c) To achieve better vibration isolation performance, the stiffness coefficients of the QZS isolator should be reduced to small. This would result in very low loading capacity. However, for the SLS-VI platform, it can be designed to have sufficient stiffness to support a desired weight but maintaining a very competitive vibration isolation performance, because (c1) the linear stiffness is not necessarily to be zero (compared with the QZS isolator in (28)); (c2) several structural parameters such as n , θ and l can be used to tune the equivalent stiffness of the system conveniently. Importantly, to achieve a better performance for the SLS-VI platform, the damping coefficients c_1 – c_3 can all be used easily for performance improvement (e.g. assembling a semi-active control device with linear damper on the left joint in the bottom layer of the platform).

4. Analysis of equivalent stiffness and damping

To understand more about the nonlinear mechanism of the SLS-VI platform in vibration control and its relationship with structural parameters, the equivalent stiffness and damping are investigated in this section. The equivalent stiffness and damping can be obtained by the stiffness function and damping function f_1, f_2, f_3 in dynamical equation.

4.1. Equivalent stiffness

The overall spring force of the isolation platform is given in (19), which is obviously a nonlinear function, and from which the equivalent linear and nonlinear stiffness coefficients $\beta_1, \beta_2, \beta_3$ and β_4 can be obtained, which are listed in Appendix B.

The linear stiffness coefficient β_1 is a dominant factor to represent the resonant frequency of the system. To have a better vibration isolation performance, this coefficient should obviously be reduced in order to have a low resonant frequency. From the dimensionless transform of coefficients and (B.1), the dimensionless resonant frequency of the system is

$$\omega_2 = \sqrt{\frac{\beta_1}{k_l}} = \frac{\tan \theta}{n} \tag{29}$$

With (29), the resonant frequency for different assembly angle θ and number of layer n is shown in Fig. 12.

From Fig. 12, the dimensionless resonant frequency ω_2 extremely depends on the structural parameters n and θ . It shows that increasing n or decreasing θ can both reduce the resonant frequency and thus improve isolation performance.

The nonlinear stiffness coefficients can actually influence not only the displacement transmissibility but also the vibration offset of the platform. The three coefficients β_2, β_3 and β_4 for different structural parameters are shown in Fig. 13.

From Fig. 13, it can be seen that as n or l decrease or θ increases, the nonlinear coefficients β_2, β_3 and β_4 increase. Considering the results in Section 3, the increase of the nonlinear coefficients is helpful to vibration suppression but also incurs more vibration offset.

It can also be seen that the sensitivities of the three coefficients above are more differentiable with respect to the parameter l in a large value range for a smaller n , and basically very different with different structural parameters. The different sensitivity of the stiffness coefficients with respect to different structural parameters provides potentially an effective way for optimal design or realization (in a passive way) of a desired nonlinear stiffness characteristic for the SLS-VI system, which would be of great significance to engineering practice. This will be further investigated in a future study.

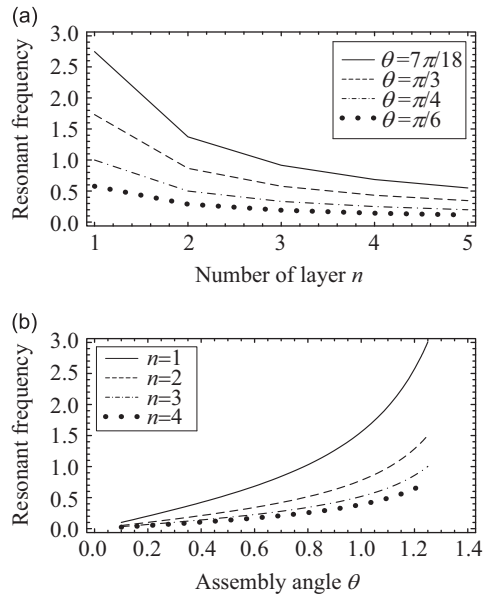


Fig. 12. The value of resonant frequency ω_2 (a) for different number of layer n ; and (b) different assembly angle θ .

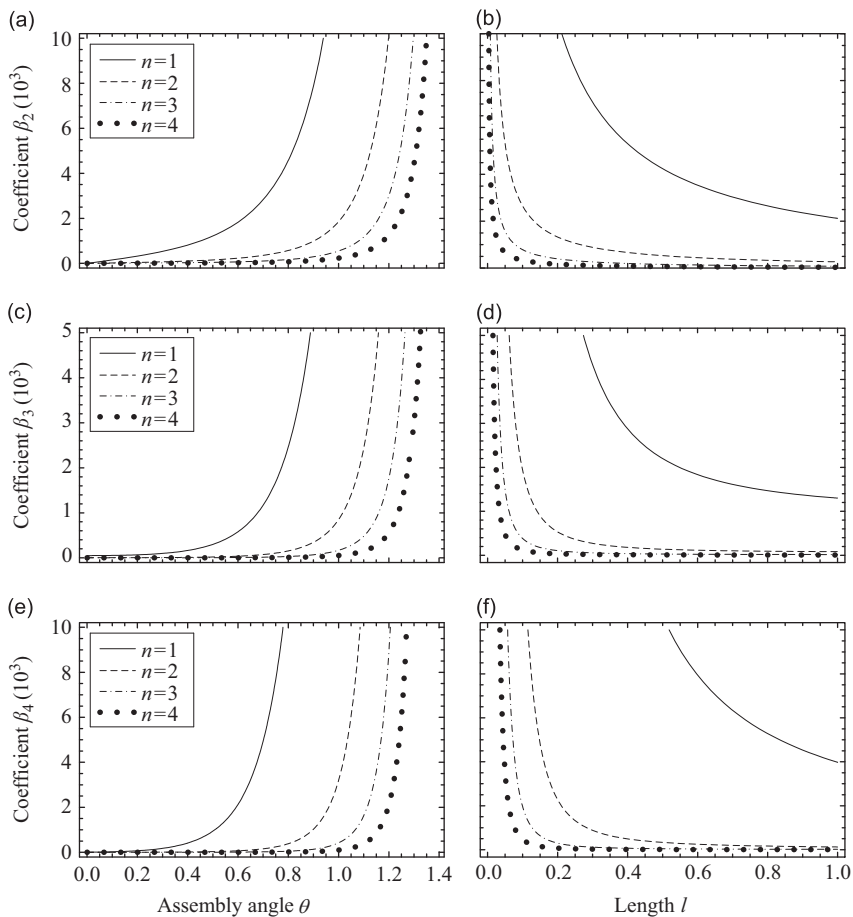


Fig. 13. The values of nonlinear coefficients β_2, β_3 and β_4 (a) value of β_2 for different n and θ ; (b) value of β_2 for different n and l ; (c) value of β_3 for different n and θ ; (d) value of β_3 for different n and l ; (e) value of β_4 for different n and θ ; (f) value of β_4 for different n and l .

4.2. Equivalent damping

The Taylor series expansions of the damping forces due to rotational and horizontal friction are shown in (20) and (21). The overall damping force of the system can be written as

$$f'_d(\dot{y}) = c_1\dot{y} + n_x c_2(\zeta_0 + \zeta_1\dot{y} + \zeta_2\dot{y}^2)\dot{y} + c_3(\zeta_3 + \zeta_4\dot{y} + \zeta_5\dot{y}^2)\dot{y} \\ = (c_1 + n_x c_2 \zeta_0 + c_3 \zeta_3)\dot{y} + (n_x c_2 \zeta_1 + c_3 \zeta_4)\dot{y}^2 + (n_x c_2 \zeta_2 + c_3 \zeta_5)\dot{y}^3 \quad (30)$$

where the coefficients $\zeta_0, \zeta_1, \zeta_2, \zeta_3, \zeta_4, \zeta_5; c_1, c_2, c_3;$ and n_x are given as before. Obviously, this is also a nonlinear function. Define $\zeta_l, \zeta_{n1},$ and ζ_{n2} as the coefficients of the overall damping force in (30) as $\zeta_l = c_1 + n_x c_2 \zeta_0 + c_3 \zeta_3, \zeta_{n1} = n_x c_2 \zeta_1 + c_3 \zeta_4,$ and $\zeta_{n2} = n_x c_2 \zeta_2 + c_3 \zeta_5,$ which can be further written as

$$\zeta_l = C_{nx} \cdot \zeta_{0,3}, \zeta_{n1} = C_{nx} \cdot \zeta_{1,4}, \zeta_{n2} = C_{nx} \cdot \zeta_{2,5} \quad (31)$$

where $C_{nx} = [c_1 \ n_x c_2 \ c_3], \zeta_{0,3} = [1, \zeta_0, \zeta_3]^T, \zeta_{1,4} = [0, \zeta_1, \zeta_4]^T, \zeta_{2,5} = [0, \zeta_2, \zeta_5]^T.$ Then Eq. (30) can be written as

$$f'_d(\dot{y}) = C_{nx}(\zeta_{0,3} + \zeta_{1,4}\dot{y} + \zeta_{2,5}\dot{y}^2)\dot{y} \quad (32)$$

It can be seen that (32) presents a nonlinear damping force which is not only a function of velocity but also depends on the displacement, and the coefficients of this damping force are functions of structural parameters. It is clear that $\zeta_{0,3}, \zeta_{1,4}$ and $\zeta_{2,5}$ are symbolically independent. Therefore, the equivalent damping coefficient in (32) can be designed (by adjusting structural parameters) to any nonlinear function that can be approximated by the second degree polynomial in terms of $\dot{y}.$ This definitely provides potentially an effective method for nonlinear damping design in a passive manner, which is of great interest to engineering practice [12] and will be investigated further.

The values of the three damping coefficients ζ_l, ζ_{n1} and ζ_{n2} for different parameters are shown in Fig. 14.

From Fig. 14, $\zeta_l, \zeta_{n1},$ and ζ_{n2} increase with the decrease of $n,$ the increase of $\theta,$ and decrease of $l.$ Also, the damping coefficients are linear increasing functions of $c_3.$ Thus increasing c_3 can reduce the displacement transmissibility at around resonant frequency.

More specifically, it is clear that the linear damping coefficient ζ_l is dependent on c_1 while the nonlinear damping coefficients ζ_{n1} and ζ_{n2} are unrelated with $c_1.$ Therefore, the value of ζ_l can be adjusted by different c_1 independently. The value of ζ_l is shown in Fig. 15 for different value of c_1, n and $l.$

From Fig. 15, it is easy to see that, as c_1 increases, the value of ζ_l is raised. The increase of ζ_l is helpful for isolation at around resonant frequency but increase the vibration at high frequencies. When the linear damping is reduced for high

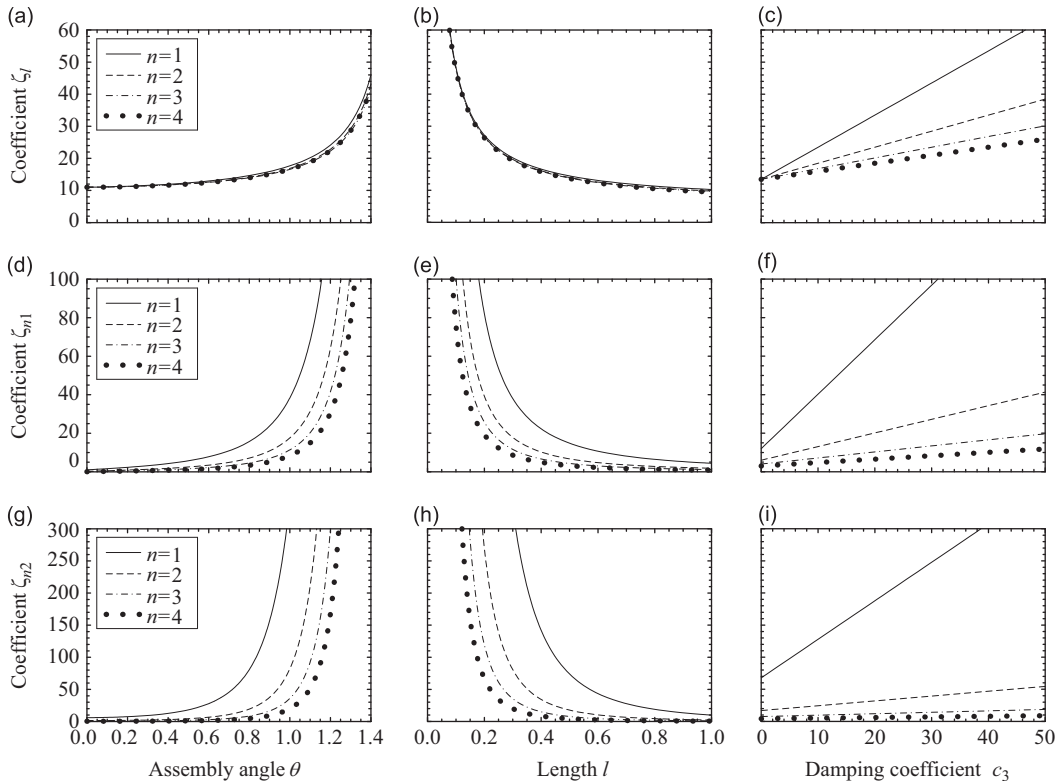


Fig. 14. The value of damping coefficients ζ_l, ζ_{n1} and ζ_{n2} . The value of ζ_l is shown in (a) for $l=0.5, c_3=1;$ (b) for $\theta=\pi/4, c_3=1;$ (c) for $l=0.5, \theta=\pi/4.$ The value of ζ_{n1} is shown in (d) for $l=0.5, c_3=1;$ (e) for $\theta=\pi/4, c_3=1;$ (f) for $l=0.5, \theta=\pi/4.$ The value of ζ_{n2} is shown in (g) for $l=0.5, c_3=1;$ (h) for $\theta=\pi/4, c_3=1;$ (i) for $l=0.5, \theta=\pi/4.$

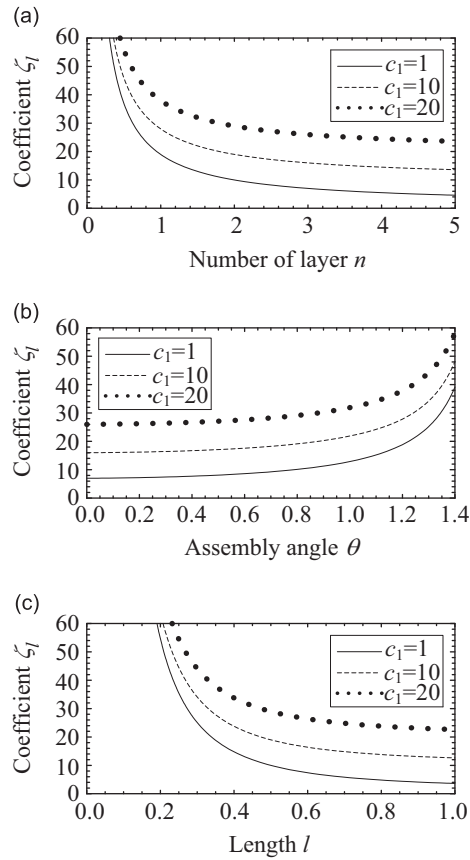


Fig. 15. The value of linear damping coefficient ζ_l . (a) for $\theta=\pi/4, l=0.5$; (b) for $n=2, l=0.5$; (c) for $n=2, \theta=\pi/4$.

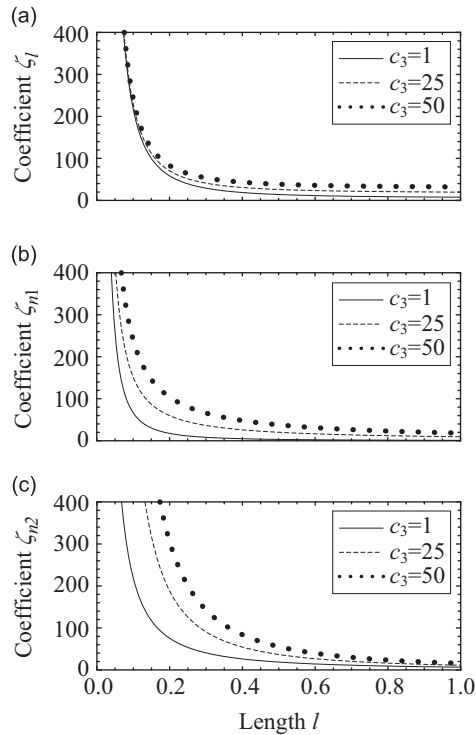


Fig. 16. The value of coefficients of damping for different c_3 and l . (a) Linear damping coefficient ζ_l ; (b) nonlinear damping coefficient ζ_{n1} ; and (c) nonlinear damping coefficient ζ_{n2} .

frequency performance, nonlinear damping must be used for low frequency vibration isolation around resonant frequency [12–14]. Fortunately, the nonlinear damping force in (32) provides sufficient capability to achieve such an advantageous damping system (see also Appendix B).

It should be noted that, although there are coupling effects between nonlinear damping coefficients ζ_{n1} , and ζ_{n2} when tuning the same structural parameters, an optimization could solve this problem since the sensitivities of those coefficients with respect to different structure parameters are very different. For example, consider the linear and nonlinear damping coefficients in (30) for different c_3 and l which are shown in Fig. 16.

From Fig. 16, the value of ζ_l for $c_3=1$, $c_3=25$, and $c_3=50$ are very close while nonlinear coefficients ζ_{n1} and ζ_{n2} change quite different as c_3 increase.

5. Conclusions

A nonlinear vibration isolation system, i.e., SLS-VI, is proposed and studied in this paper. The SLS-VI platform takes a simple scissor-like structure and can achieve very advantageous nonlinear vibration isolation/suppression performance by employing passive spring or damping components. By designing structural parameters, the platform can realize quasi-zero stiffness property with much better loading capacity and equilibrium stability compared with existing QZS isolators in the literature. Importantly, with only linear spring and/or damper components, the SLS-VI demonstrates very beneficial nonlinear stiffness and damping characteristics in vibration isolation, compared with traditional mass–spring–damper systems of the same equivalent springs and dampers. The platform provides novel insights into passive design of nonlinear stiffness and/or damping properties for vibration isolation/control in engineering practice.

In practice, the SLS-VI can meet different stiffness and damping requirement for different types of excitations and working conditions by designing structural parameters (e.g., n , l , θ). From the theoretical analysis results of this study, it can be seen that there is no an obvious priority list to design those structural parameters. The sensitivities of equivalent stiffness and damping properties of the system with respect to different structure parameters are very different. This presents the possibility for different stiffness and damping design, and also indicates that an optimization process can be employed for a detailed engineering task (considering the actual requirements on performance, size, weight, frictions and others).

The SLS system will be further studied by considering mass and flexibility of connecting rods in system modeling, validating the theoretical results with a practical experimental platform, investigating the optimal design of structural parameters and exploring the most potential value of the SLS platform in 3D vibration control.

Acknowledgment

The authors would like to thank the useful comments and constructive suggestions from the handling editor and anonymous reviewers, which do improve the quality of the manuscript. The authors also gratefully acknowledge the support from a NSFC project (No. 61374041) of China, a GRF project (Ref. 517810) of Hong Kong RGC, Department General Research Funds and internal Competitive Research Grants of Hong Kong Polytechnic University, and the other two NSFC projects of China (Refs. 11272236 and 11032009).

Appendix A

See Tables 1–5.

Table 1
The structural parameters of the SLS-VI.

| Symbol | Structural parameters | Unit |
|----------|--|-----------------------|
| k_1 | Linear stiffness | N m^{-1} |
| k_n | Nonlinear stiffness | N m^{-3} |
| M | Mass of isolation object | kg |
| n | Number of layer | |
| n_x | Number of joints | |
| l | Length of connecting rod | m |
| θ | Assembly angle of connecting rod | rad |
| c_1 | Air damping coefficient | N s m^{-1} |
| c_2 | Damping coefficient of rotational friction | N s rad^{-1} |
| c_3 | Damping coefficient of horizontal friction | N s m^{-1} |

Table 2
The motion and variables of SLS-VI.

| Symbol | Structural parameters | Unit |
|------------|--|---------------------|
| y | Absolute motion of isolation object | m |
| z | Base excitation | m |
| \hat{y} | Relative motion of isolation object and base | m |
| φ | Rotation transport motion | rad |
| x | Horizontal transport motion | m |
| z_0 | Amplitude of base excitation z | m |
| ω_0 | Frequency of base excitation z | rad s ⁻¹ |
| a_0 | Offset of vibration \hat{y} | |
| a | Amplitude of relative motion \hat{y} | |
| ϕ | Phase of relative motion \hat{y} | |
| T_d | Displacement transmissibility | |

Table 3
The dimensionless transfer of SLS-VI.

| Dimensionless parameters | Value |
|--------------------------|--|
| ω_1 | $\sqrt{\frac{k_1}{M}}$ |
| t' | $\omega_1 t$ |
| ω_2 | $\sqrt{\frac{\beta}{k_1}}$ |
| γ_1 | β_2/k_1 |
| γ_2 | β_3/k_1 |
| γ_3 | β_4/k_1 |
| ξ_1 | $\frac{c_1 + \beta_2 c_{20} + c_{33}}{2\sqrt{Mk_1}}$ |
| ξ_2 | $\frac{\beta_2 c_{21} + c_{34}}{2\sqrt{Mk_1}}$ |
| ξ_3 | $\frac{\beta_2 c_{22} + c_{35}}{2\sqrt{Mk_1}}$ |
| Ω | ω_0/ω_1 |

Table 4
The dimensionless transfer of mass-spring-damping isolator.

| Dimensionless parameters | Value |
|--------------------------|----------------------------|
| ω_1 | $\sqrt{\frac{k_1}{M}}$ |
| t' | $\omega_1 t$ |
| γ_1 | k_n/k_1 |
| ξ_1 | $\frac{c_1}{2\sqrt{Mk_1}}$ |
| Ω | ω_0/ω_1 |

Table 5
The dimensionless transfer of quasi-zero-stiffness isolator.

| Dimensionless parameters | Value |
|--------------------------|----------------------------|
| ω_1 | $\sqrt{\frac{k_1}{M}}$ |
| t' | $\omega_1 t$ |
| γ | k_n/k_1 |
| ξ_1 | $\frac{c_1}{2\sqrt{Mk_1}}$ |
| Ω | ω_0/ω_1 |

Appendix B

The expression of β_1 , β_2 , β_3 , β_4 , ζ_0 , ζ_1 , ζ_2 , ζ_3 , ζ_4 , and ζ_5 in (19–21) are as follows:

$$\beta_1 = \frac{k_l \tan^2 \theta}{n^2} \quad (\text{B.1})$$

$$\beta_2 = \frac{3k_l \sec^4 \theta \sin \theta}{4n^3 l} \quad (\text{B.2})$$

$$\beta_3 = \frac{k_n}{n^4} - \frac{4(k_l + 2k_n l^2 \cos 2\theta) \sec^3 \theta - 5k_l \sec^5 \theta}{8n^4 l^2 \cos \theta} \quad (\text{B.3})$$

$$\beta_4 = \frac{5 \sin \theta (5k_l + 2k_n l^2 - 2k_l \cos 2\theta - 2k_n l^2 \cos 4\theta)}{64n^5 l^3 \cos^8 \theta} \quad (\text{B.4})$$

$$\zeta_0 = \frac{1}{2nl \cos \theta} \quad (\text{B.5})$$

$$\zeta_1 = \frac{\sin \theta}{4n^2 l^2 \cos^3 \theta} \quad (\text{B.6})$$

$$\zeta_2 = \frac{(2 - \cos 2\theta)}{16n^3 l^3 \cos^5 \theta} \quad (\text{B.7})$$

$$\zeta_3 = \frac{\tan \theta}{n} \quad (\text{B.8})$$

$$\zeta_4 = \frac{1}{2n^2 l \cos^3 \theta} \quad (\text{B.9})$$

$$\zeta_5 = \frac{3 \sin \theta}{8n^3 l^2 \cos^5 \theta} \quad (\text{B.10})$$

Appendix C

The equations for a_0 , a and ϕ of the response of SLS-VI obtained by the HBM are as follows:

$$a_0^2 \gamma_1 + \frac{a^2 \gamma_1}{2} + a_0^3 \gamma_2 + \frac{3}{2} a_0 a^2 \gamma_2 + a_0^4 \gamma_3 + 3a_0^2 a^2 \gamma_3 + \frac{3a^4 \gamma_3}{8} + a_0 \omega_2^2 = 0 \quad (\text{C.1})$$

$$\begin{aligned} & (2a\xi_1 \Omega + 2a_0 a \Omega + 2a_0^2 a \xi_3 \Omega + \frac{1}{2} a^3 \xi_3 \Omega) \cos \phi \\ & + a(2a_0 \gamma_1 + 3a_0^3 \gamma_2 + 4a_0^3 \gamma_3 - \Omega^2 + \omega_2^2) \sin \phi + a^3 \left(\frac{3}{4} \gamma_2 + 3a_0 \gamma_3 \right) \sin \phi = 0 \end{aligned} \quad (\text{C.2})$$

$$\begin{aligned} & (2a_0 a \gamma_1 + 3a_0 a \gamma_2 + \frac{3}{4} a^3 \gamma_2 + 4a_0^3 a \gamma_3 + 3a_0 a^3 \gamma_3) \cos \phi \\ & - a(2\xi_1 \Omega + 2a_0 \xi_2 \Omega + 2a_0^2 \xi_3 \Omega + \Omega^2 - \omega_2^2) \sin \phi + \frac{1}{2} a^3 \xi_3 \Omega \sin \phi + z_0 \Omega^2 = 0 \end{aligned} \quad (\text{C.3})$$

References

- [1] W.S. Robertson, M.R.F. Kidner, B.S. Cazzolato, A.C. Zander, Theoretical design parameters for a quasi-zero stiffness magnetic spring for vibration isolation, *Journal of Sound and Vibration* 326 (1–2) (2009) 88–103, <http://dx.doi.org/10.1016/j.jsv.2009.04.015>.
- [2] J.Z. Zhang, D. Li, S. Dong, An ultra-low frequency parallel connection nonlinear isolator for precision instruments., *Key Engineering Materials* 257–258 (2004) 231–236. (doi: 10.4028 /KEM.257-258.231).
- [3] K. Denoyer, C. Johnson, *Recent achievements in vibration isolation systems for space launch and on-orbit applications*, 52nd International Astronautical Congress, , 2001, 1–11.
- [4] A. Carella, M.J. Brennan, T.P. Waters, Static analysis of a passive vibration isolator with quasi-zero-stiffness characteristic, *Journal of Sound and Vibration* 301 (3–5) (2007) 678–689, <http://dx.doi.org/10.1016/j.jsv.2006.10.011>.
- [5] I. Kovacic, M.J. Brennan, T.P. Waters, A study of a nonlinear vibration isolator with a quasi-zero-stiffness characteristic, *Journal of Sound and Vibration* 315 (3) (2008) 700–711, <http://dx.doi.org/10.1016/j.jsv.2007.12.019>.
- [6] A. Carella, M.J. Brennan, T.P. Waters, Optimization of a quasi-zero-stiffness isolator, *Journal of Mechanical Science and Technology* 21 (6) (2007) 946–949, <http://dx.doi.org/10.1007/BF03027074>.

- [7] A. Carrella, M.J. Brennan, I. Kovacic, T.P. Waters, On the force transmissibility of a vibration isolator with quasi-zero-stiffness, *Journal of Sound and Vibration* 322 (4–5) (2009) 707–717, <http://dx.doi.org/10.1016/j.jsv.2008.11.034>.
- [8] G. Gatti, I. Kovacic, M.J. Brennan, On the response of a harmonically excited two degree-of-freedom system consisting of a linear and a nonlinear quasi-zero stiffness oscillator, *Journal of Sound and Vibration* 329 (10) (2010) 1823–1835, <http://dx.doi.org/10.1016/j.jsv.2009.11.019>.
- [9] A. Carrella, M.J. Brennan, T.P. Waters, V. Lopes Jr, Force and displacement transmissibility of a nonlinear isolator with high-static-low-dynamic-stiffness, *International Journal of Mechanical Sciences* 55 (1) (2012) 22–29, <http://dx.doi.org/10.1016/j.ijmecsci.2011.11.012>.
- [10] T.D. Le, K.K. Ahn, A vibration isolation system in low frequency excitation region using negative stiffness structure for vehicle seat, *Journal of Sound and Vibration* 330 (26) (2011) 6311–6335, <http://dx.doi.org/10.1016/j.jsv.2011.07.039>.
- [11] H.J. Ahn, Performance limit of a passive vertical isolator using a negative stiffness mechanism, *Journal of Mechanical Science and Technology* 22 (2008) 2357–2364, <http://dx.doi.org/10.1007/s12206-008-0930-7>.
- [12] Z.L. Xiao, X.J. Jing, L. Cheng, The transmissibility of vibration isolators with cubic nonlinear damping under both force and base excitations, *Journal of Sound and Vibration* 332 (5) (2013) 1335–1354, <http://dx.doi.org/10.1016/j.jsv.2012.11.001>.
- [13] X.J. Jing, Z.Q. Lang, S.A. Billings, Nonlinear influence in the frequency domain: Alternating series, *Systems and Control Letters* 60 (5) (2011) 295–309, <http://dx.doi.org/10.1016/j.sysconle.2011.01.003>.
- [14] X.J. Jing, Z.Q. Lang, S.A. Billings, Frequency Domain Analysis for Suppression of Output Vibration from Periodic Disturbance using Nonlinearities, *Journal of Sound and Vibration* 314 (2008) 536–557, <http://dx.doi.org/10.1016/j.jsv.2008.01.031>.
- [15] Y. Sato, S. Umebara, Power-saving magnetization for magnetorheological fluid control using a combination of permanent magnet and electromagnet, *IEEE Transactions on Magnetics* 48 (11) (2012) 3521–3524, <http://dx.doi.org/10.1109/TMAG.2012.2207093>.
- [16] G.Z. Yao, Y. Qiu, Vibration control of a rotor system by disk type electrorheological damper, *Journal of Sound and Vibration* 219 (1) (1999) 175–188, <http://dx.doi.org/10.1006/jsvi.1998.1852>.
- [17] X.C. Zhu, X.J. Jing, L. Cheng, Magnetorheological fluid dampers: a review on structure design and analysis, *Journal of Intelligent Material Systems and Structures* 23 (8) (2012) 839–873, <http://dx.doi.org/10.1177/1045389x12436735>.
- [18] X.C. Zhu, X.J. Jing, L. Cheng, Systematic design of a magneto-rheological fluid embedded pneumatic vibration isolator subject to practical constraints, *Smart Materials and Structures* 21 (3) (2012) 035006, <http://dx.doi.org/10.1088/0964-1726/21/3/035006>.
- [19] M. Zapateiro, F. Pozo, H.R. Karimi, N.S. Luo, Semiactive control methodologies for suspension control with magnetorheological dampers, *IEEE Transactions on Mechatronics* 17 (2) (2012) 370–380, <http://dx.doi.org/10.1109/TMECH.2011.2107331>.
- [20] J.H. Jung, T.H. Cheng, I.K. Oh, Electromagnetic synchronized switch damping for vibration control of flexible beams, *IEEE Transactions on Mechatronics* 17 (6) (2012) 1031–1038, <http://dx.doi.org/10.1109/TMECH.2011.2157934>.
- [21] J.M. Rodriguez-Fortun, J. Orus, J. Alfonso, F.B. Gimeno, J.A. Castellanos, Flatness-based active vibration control for piezoelectric actuator, *IEEE Transactions on Mechatronics* 18 (1) (2013) 221–229, <http://dx.doi.org/10.1109/TMECH.2011.2166998>.
- [22] M. Zapateiro, N. Luo, H.R. Karimi, J. Vehi, Vibration control of a class of semiactive suspension system using neural network and backstepping techniques, *Mechanical Systems and Signal Processing* 23 (6) (2009) 1946–1953, <http://dx.doi.org/10.1016/j.ymssp.2008.10.003>.
- [23] H.R. Karimi, H.J. Gao, H.∞ LMI-based, synchronization of second-order neutral master–slave systems using delayed output feedback control, *International Journal of Control, Automation, and Systems* 7 (3) (2009) 371–380, <http://dx.doi.org/10.1007/s12555-009-0306-5>.
- [24] H.Y. Li, H.H. Liu, H.J. Gao, P. Shi, Reliable fuzzy control for active suspension systems with actuator delay and fault, *IEEE Transactions on Fuzzy Systems* 20 (2) (2012) 342–357, <http://dx.doi.org/10.1109/TFUZZ.2011.2174244>.
- [25] S.J. Huang, K.S. Huang, K.C. Chiou, Development and application of a novel radial basis function sliding mode controller, *Mechatronics* 13 (2003) 313–329, [http://dx.doi.org/10.1016/S0957-4158\(01\)00050-2](http://dx.doi.org/10.1016/S0957-4158(01)00050-2).
- [26] X.J. Jing, Z.Q. Lang, S.A. Billings, Output frequency properties of nonlinear systems, *International Journal of Non-Linear Mechanics* 45 (7), 681–690, <http://dx.doi.org/10.1016/j.ijnonlinmec.2010.04.002>.
- [27] N. Olgac, B.T. Holm-Hansen, A novel active vibration absorption technique: delayed resonator, *Journal of Sound and Vibration* 176 (1) (1994) 93–104, <http://dx.doi.org/10.1006/jsvi.1994.1360>.
- [28] N. Olgac, B.T. Holm-Hansen, Design considerations for delayed-resonator vibration absorbers, *Journal of Engineering Mechanics* 121 (1) (1995) 80–89, [http://dx.doi.org/10.1061/\(ASCE\)0733-9399\(1995\)121:1\(80\)](http://dx.doi.org/10.1061/(ASCE)0733-9399(1995)121:1(80)).
- [29] N. Olgac, M. Hosek, Active vibration absorption using delayed resonator with relative position measurement, *Journal of Vibration and Acoustics* 119 (1) (1997) 131–136, <http://dx.doi.org/10.1115/1.2889680>.
- [30] Y.Y. Zhao, J. Xu, Effects of delayed feedback control on nonlinear vibration absorber system, *Journal of Sound and Vibration* 308 (1–2) (2007) 212–230, <http://dx.doi.org/10.1016/j.jsv.2007.07.041>.
- [31] B. Bhikkaji, S.O.R. Moheimani, I.R. Petersen, A negative imaginary approach to modeling and control of a collocated structure, *IEEE Transactions on Mechatronics* 17 (4) (2012) 717–727, <http://dx.doi.org/10.1109/TMECH.2011.2123909>.
- [32] I. Maciejewski, L. Meyer, T. Krzyzynski, Modelling and multi-criteria optimisation of passive seat suspension vibro-isolating properties, *Journal of Sound and Vibration* 324 (3–5) (2009) 520–538, <http://dx.doi.org/10.1016/j.jsv.2009.02.021>.
- [33] I. Maciejewski, L. Meyer, T. Krzyzynski, The vibration damping effectiveness of an active seat suspension system and its robustness to varying mass loading, *Journal of Sound and Vibration* 329 (19) (2010) 3898–3914, <http://dx.doi.org/10.1016/j.jsv.2010.04.009>.
- [34] A.H. Nayfeh, D.T. Mook, *Nonlinear Oscillations*, Wiley-Interscience, New York, 1979.